

Intelligent Controlled Three-Phase Squirrel-Cage Induction Generator System Using Hybrid Wavelet Fuzzy Neural Network

Faa-Jeng Lin, and Jin-Kuan Chang

Abstract—An intelligent controlled three-phase squirrel-cage induction generator (SCIG) system for grid-connected wind power applications using hybrid wavelet fuzzy neural network (WFNN) is proposed in this study. First, the indirect field-oriented mechanism is implemented for the control of the SCIG system. Then, an AC/DC power converter and a DC/AC power inverter are developed to convert the electric power generated by a three-phase SCIG to power grid. Moreover, the dynamic model of the SCIG system and an ideal computed torque controller are developed for the control of the square of DC-link voltage. Furthermore, an intelligent hybrid WFNN controller and two WFNN controllers, which are computation intensive approaches, are proposed for the AC/DC power converter and the DC/AC power inverter respectively to improve the transient and steady-state responses of the SCIG system at different operating conditions. In the intelligent hybrid WFNN controller, to relax the requirement of the lumped uncertainty in the design of the ideal computed torque controller, a WFNN is designed as an uncertainty observer to adapt the lumped uncertainty online. Finally, the feasibility and effectiveness of the SCIG system for grid-connected wind power applications is verified with experimental results.

I. INTRODUCTION

Owing to the concern of sustainable environment, there is much interest in renewable energy resources of electrical power generation. The most promising one is wind energy and wind turbines have been utilized vastly to exploit this energy source to directly generate electrical power [1]. According to the Global Wind Energy Council, about 41GW of wind energy has been installed in 2011, bringing the total installed capacity globally to more than 237GW at the end of 2011. Thus, wind energy is recognized worldwide as a cost-effective, environmental friendly solution to energy shortages, and it is expected to be capable of becoming a major resource to the world's electricity supply in the near future [2], [3].

In general, the SCIG system can be represented by a nonlinear model. Therefore, the feedback linearization technique can be applied to transform the SCIG system model into an equivalent model with simpler form. Although the dynamic model of the SCIG system is simplified, only the nominal system parameters are considered in feedback linearization design. This usually leads to the problems of deteriorated performance and instability since the system parameters are usually varied with different operating

conditions. As a result, the development of high performance controllers based on this simplified model is very difficult to complete. On the other hand, the control of DC-link voltage is very critical for the control of renewable energy resources. Therefore, in this study, the derivation of the SCIG dynamic model is based on the control of the DC-link voltage.

The fuzzy neural network (FNN) possesses the following three advantages: 1. the capability of artificial neural networks in learning from processes; 2. the capability of fuzzy reasoning in handling uncertain information; 3. the ability to approximate uncertainties and nonlinear systems and do not require mathematical models [4]. Thus, there were many researches which use FNNs to represent complex plants and construct advanced controllers based on the backpropagation (BP) learning algorithm [5]. Furthermore, the wavelet neural networks (WNNs) can converge quickly and have high precision with reduced network size owing to the time–frequency localization properties of wavelets [6]. Due to the above advantages of the FNN and the WNN, the WFNN proposed in [7], which combines the advantages of FNN and WNN, is adopted to improve the transient and steady-state responses of the SCIG system at different operating conditions in this study. However, the proof of stability of the WFNN control system was not provided in [7].

A grid-connected three-phase SCIG system with intelligent hybrid WFNN control is investigated in this study for wind power applications. First, an indirect field-oriented controlled SCIG system with an AC/DC power converter and a DC/AC power inverter is developed to convert the electric power generated by the three-phase SCIG to power grid. Then, the dynamic model of the SCIG system where the square of DC-link voltage is the control variable and an ideal computed torque controller are developed for the control of the square of DC-link voltage. However, in the design of ideal computed torque controller, the required lumped uncertainty is unknown in practical application. Therefore, an intelligent hybrid WFNN controller is proposed for the AC/DC power converter to improve the transient and steady-state responses of the SCIG system at different operating conditions. In the hybrid WFNN controller, a WFNN is designed as an uncertainty observer and a compensated controller compensates the minimum approximation error of the observer. Moreover, the design of the hybrid WFNN controller is based on Lyapunov stability. Furthermore, the adaptation law of the WFNN is modified by using a projection algorithm to ensure the convergence of the WFNN. In addition, since the dynamic model of the power grid is unavailable, two WFNN controllers are proposed for the grid-connected DC/AC power inverter for the control of

F. J. Lin is with the Department of Electrical Engineering, National Central University, Chungli 320, Taiwan (corresponding author to provide phone: 886-3-4227151 ext.34532; e-mail: linfj@ee.ncu.edu.tw).

J. K. Chang is with the Department of Electrical Engineering, National Central University, Chungli 320, Taiwan.

active and reactive power.

II. INDIRECT FIELD-ORIENTED CONTROLLED SCIG SYSTEM

The SCIG is controlled in a synchronously rotating reference frame with the d -axis oriented along the rotor-flux vector position in this study. Therefore, a decoupled control between the rotor excitation current and the electrical torque is obtained. The model of the SCIG represented in the synchronously rotating reference frame can be found in [8]. According to the indirect field-oriented control, the rotor flux in the d -axis can be controlled by using d -axis stator current i_{ds} . Moreover, the electromagnetic torque can be simplified to

$$T_e = \frac{3P_M}{4} \frac{L_m^2}{L_r} i_{ds} i_{qs} = K_t i_{qs} \quad (1)$$

where T_e is the electromagnetic torque; P_M is the pole number; L_m and L_r are the mutual inductance and rotor inductance; i_{qs} is the q -axis stator current; torque constant is defined as $K_t = 3P_M L_m^2 i_{ds} / (4L_r)$.

The block diagram of the control strategy and power circuit of the SCIG system is shown in Fig. 1. The prime mover, which adopted the permanent-magnet synchronous motor (PMSM), is directly coupled to the SCIG and emulates the operation of the wind turbine. The variable-voltage variable-frequency power generated by the SCIG is rectified to DC power by an AC/DC power converter. The AC/DC power converter also supplies lagging excitation current to the SCIG. Moreover, the AC/DC power converter is used mainly to control the square of DC-link voltage. The electric angular angle θ_e is obtained by using the indirect field-oriented control. The square of DC-link voltage error is sent to the hybrid WFNN controller, and the torque control current i_{qs}^* is then generated. Furthermore, the DC power is converted to a constant-voltage constant-frequency AC power, which is 60Hz 110Vrms, by a DC/AC power inverter and following by a three-phase 110Vrms/220Vrms transformer for three-phase power grid. The DC/AC power inverter is designed for the control of the active and reactive

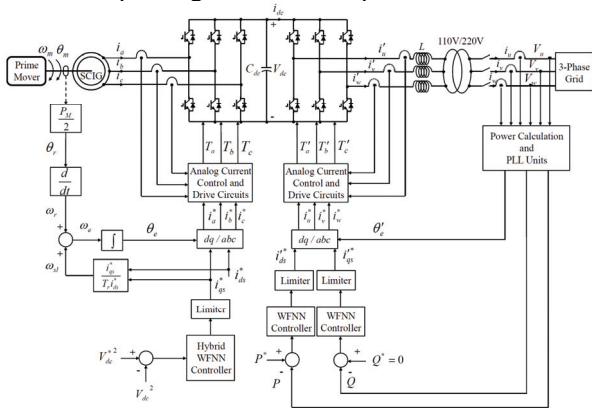


Fig. 1. System configuration of SCIG system using power converters.

power error are sent to the WFNN controllers, and the active power control current i_{ds}^* and reactive power control current i_{qs}^* are generated.

III. WIND TURBINE EMULATOR

In this study, the PMSM servo drive is adopted as the prime mover to emulate the wind turbine. Moreover, according to the actual wind speed distribution, various wind speeds $v=6, 8, 10, 12$ m/s are selected to obtain the optimal rotor speeds of the generator as show in Fig. 2 based on the optimal tip speed ratio. Furthermore, the power-speed characteristics shown in Fig. 2(a) for a 2kW three-blade horizontal axis wind turbine with diameter of 2.4m is obtained using the wind turbine model at various wind speeds. From Fig. 2(a), the shaft power of the wind turbine is related to its wind speed v and rotor speed rpm. In practice, a simplified form of power performance coefficient and tip speed ratio ($C_p - \lambda$) as shown in Fig. 2(b) can also represent the characteristics of a wind turbine. The relationship of the tip speed ratio can be described as follows [9]:

$$\lambda = \frac{R_m \omega_m}{v} \quad (2)$$

where R_m is the turbine rotor radius in meter; λ is the tip ratio. Choosing the optimal $\lambda_{opt} = 5.52$, for the maximum power coefficient $C_{p \max} = 0.436$ at a given wind speed, the maximum power can be extracted by setting the reference mechanical rotor speed as follows [8]:

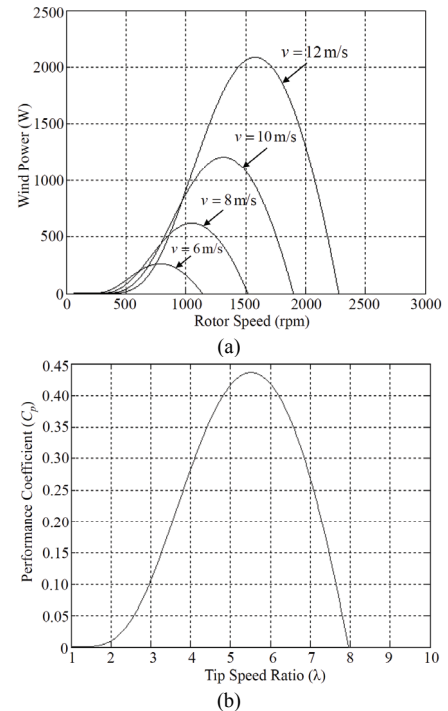


Fig. 2. (a) Power-speed characteristics of wind turbine, (b) $C_p - \lambda$ characteristic of wind turbine.

$$\omega_m^* = \frac{\lambda_{opt} v}{R_m} \quad (3)$$

Furthermore, the power-speed characteristic of a wind turbine is implemented by the field-oriented control PMSM servo drive. Therefore, in order to emulate the wind variation in grid-connected application, a speed control loop is adopted to regulate the rotor speed with the corresponding wind speed to obtain the maximum power output of the wind turbine.

IV. INTELLIGENT HYBRID WFNN CONTROLLER

A. Dynamic Analysis of SCIG System

The dynamic equation of rotation by the prime mover with SCIG as shown in Fig. 1 can be represented as follows:

$$T_m(t) - T_e(t) = J\omega_m'(t) + B\omega_m(t) \quad (4)$$

where T_m is the mechanical torque of the prime mover; J and B are the inertia and damping coefficient of the prime mover and the SCIG; $\omega_m'(t)$ is the time derivative of $\omega_m(t)$. It is assumed that there is no active power lose in both the AC/DC converter and DC/AC inverter. Then, based on the principle of power balance, the dynamics of the DC-link voltage is shown as follows:

$$\frac{C}{2}(V_{dc}^2)'(t) + P(t) = P_{SCIG}(t) = T_e(t)\omega_m(t) \quad (5)$$

where C and $V_{dc}(t)$ are the capacitor and the voltage of DC-link. Equations (6), (7) and (8) can be obtained as follows by calculating the Laplace transform of (1), (4) and (5) respectively:

$$T_e(s) = K_t i_{qs}^*(s) \quad (6)$$

$$T_m(s) - T_e(s) = (Js + B)\omega_m(s) \quad (7)$$

$$\frac{sC}{2}V_{dc}^2(s) + P(s) = P_{SCIG}(s) = T_e(s)\omega_m(s) \quad (8)$$

Substitute (6), (7) into (8), then

$$\begin{aligned} \frac{sC}{2}(Js + B)V_{dc}^2(s) &= i_{qs}^*(s)K_t T_m(s) \\ &- [i_{qs}^*(s)K_t]^2 - [Js + B]P(s) \end{aligned} \quad (9)$$

Equation (10) can be obtained as follows by (9) using the inverse Laplace transform:

$$\begin{aligned} (V_{dc}^2)''(t) &= -\frac{B}{J}(V_{dc}^2)'(t) + \frac{2}{JC}\{K_t i_{qs}^*(t) * T_m(t) \\ &- K_t^2 i_{qs}^{*2}(t) - JP'(t) - BP(t)\} \end{aligned} \quad (10)$$

where the term $i_{qs}^*(t) * T_m(t)$ is the convolution operation of $i_{qs}^*(t)$ and $T_m(t)$. To linearize $i_{qs}^*(t) * T_m(t)$ by Taylor series expansion at t_0 , the following equation can be obtained:

$$\begin{aligned} (V_{dc}^2)''(t) &= -\frac{B}{J}(V_{dc}^2)'(t) + \frac{2}{JC}\{K_t [i_{qs}^*(t) * T_m(t)]\Big|_{t=t_0} \\ &+ (i_{qs}^*(t) * T_m(t))\Big|_{t=t_0} (t-t_0) + H(t)\} - K_t^2 i_{qs}^{*2}(t) \\ &- JP'(t) - BP(t) \end{aligned} \quad (11)$$

where $H(t)$ represents high-order term of Taylor series expansion. Equation (11) can be further represented as follows:

$$\begin{aligned} (V_{dc}^2)''(t) &= -\frac{B}{J}(V_{dc}^2)'(t) + \frac{2}{JC}\{K_t [K_1 + K_2(t-t_0) \\ &+ H(t)] - K_t^2 i_{qs}^{*2}(t) - JP'(t) - BP(t)\} \end{aligned} \quad (12)$$

where K_1 and K_2 are constants. Rewrite (12) as follows:

$$(V_{dc}^2)''(t) = A(V_{dc}^2)'(t) + B(t)i_{qs}^*(t) + C(t) + D(t) \quad (13)$$

where $A = -B/J$, $B(t) = -2K_t^2 t^2 / JC$, $C(t) = \frac{2}{JC}[-JP'(t) - BP(t)]$, $D(t) = \frac{2}{JC}[K_t K_1 + K_t K_2(t-t_0) - K_t H(t)]$. Now, assume the parameters of the SCIG system are known and rewrite (13) as:

$$(V_{dc}^2)''(t) = A_n(V_{dc}^2)'(t) + B_n(t)i_{qs}^*(t) + C_n(t) + D_n(t) \quad (14)$$

Equation (14) is the nominal condition of the system, where A_n is the nominal value of A ; $B_n(t)$ is the nominal value of $B(t)$; $C_n(t)$ is the nominal value of $C(t)$; $D_n(t)$ is the nominal value of $D(t)$. If the uncertainties occur, i.e. the parameters of the system are deviated from their nominal values, the dynamic equation can be modified as:

$$\begin{aligned} (V_{dc}^2)''(t) &= (A_n + \Delta A(t))(V_{dc}^2)'(t) + (B_n(t) + \Delta B(t))i_{qs}^*(t) \\ &+ (C_n(t) + \Delta C(t)) + (D_n(t) + \Delta D(t)) \\ &= A_n(V_{dc}^2)'(t) + B_n(t)i_{qs}^*(t) + C_n(t) + W(t) \end{aligned} \quad (15)$$

where $\Delta A(t)$, $\Delta B(t)$, $\Delta C(t)$, and $\Delta D(t)$ denote the uncertainties; $W(t)$ is called the lumped uncertainty and defined as:

$$\begin{aligned} W(t) &= \Delta A(t)(V_{dc}^2)'(t) + \Delta B(t)i_{qs}^*(t) \\ &+ \Delta C(t) + D_n(t) + \Delta D(t) \end{aligned} \quad (16)$$

B. Ideal Computed Torque Controller

The proposed intelligent hybrid WFNN control system is shown in Fig. 3, where $V_{dc}^{*2}(t)$ is the square of the reference DC-link voltage; \mathbf{E} is the error vector. The intelligent hybrid WFNN controller is defined as follows:

$$i_{qs}^*(t) = U_A(t) + U_C(t) \quad (17)$$

where $U_A(t)$ is a computed torque controller and $U_C(t)$ is a compensated controller. In Fig. 3, the main tracking controller is the computed torque controller with the WFNN uncertainty observer. Moreover, the minimum approximation error of the WFNN uncertainty observer is compensated by the designed compensated controller.

The control problem is to find a control law such that the $V_{dc}^2(t)$ can track the desired trajectory $V_{dc}^{*2}(t)$ in the presence of the uncertainties. Assume the tracking error vector to be

$$\mathbf{E} = [V_{dc}^{*2}(t) \quad (V_{dc}^{*2})'(t)]^T - [V_{dc}^2(t) \quad (V_{dc}^2)'(t)]^T \quad (18)$$

$$= [e(t) \quad e'(t)]^T$$

If the lumped uncertainty of the controlled system is well known, the ideal computed torque control law can be defined as follows:

$$i_{qs}^*(t) = B_n^{-1}(t)[(V_{dc}^{*2})''(t) - A_n(V_{dc}^2)'(t) - C_n(t) - W(t) + \mathbf{K}^T \mathbf{E}] \quad (19)$$

where $\mathbf{K} = [k_2 \quad k_1]^T$; k_1 and k_2 are nonzero positive constants. Substituting (19) into (15) and using (18), the following error dynamic equation can be obtained:

$$e''(t) + k_1 e'(t) + k_2 e(t) = 0 \quad (20)$$

which implies $\lim_{t \rightarrow \infty} e(t) = 0$. Since the lumped uncertainty $W(t)$ is unknown in actual application, an WFNN uncertainty observer is proposed to estimate the value of the lumped uncertainty, which is denoted by $\hat{W}(t)$. The purpose of the uncertainty observer is to determine a value of $\hat{W}(t)$ for the computed torque controller to compel the $V_{dc}^2(t)$ to follow the desired trajectory $V_{dc}^{*2}(t)$ under the occurrence of uncertainties. Using (18), the computed torque controller is now defined as:

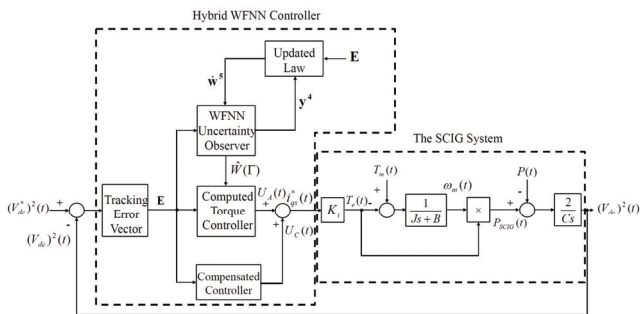


Fig. 3. Control block diagram of hybrid WFNN controller.

$$U_A(t) = B_n^{-1}(t)[(V_{dc}^{*2})''(t) - A_n(V_{dc}^2)'(t) - C_n(t) - \hat{W}(\Gamma) + \mathbf{K}^T \mathbf{E}] \quad (21)$$

where Γ are the collections of the adjustable parameters of the WFNN.

C. WFNN Uncertainty Observer

The structure of the WFNN is shown in Fig. 4 [7], including the input layer, the membership layer, the rule layer, the wavelet layer and the output layer. The basic function and signal propagation of each layer are introduced in the following:

Layer 1 (input layer):

The node input and the node output in the input layer are represented as:

$$y_i^1 = f_i^1(\text{net}_i^1(N)) = \text{net}_i^1(N), \quad i = 1, 2 \quad (22)$$

where $\text{net}_i^1(N) = x_i^1$; N represents the N th iteration; $x_1^1 = e(t)$; $x_2^1 = e'(t)$. Moreover, the input variables are $e(t) = V_{dc}^{*2}(t) - V_{dc}^2(t)$ for the square of DC-link voltage control, $e(t) = P^*(t) - P(t)$ for the active power control and $e(t) = Q^*(t) - Q(t)$ for the reactive power control.

Layer 2 (membership layer):

In the membership layer, the Gaussian function, which is adopted as the membership function, is implemented by each node. For the j th node

$$y_j^2(N) = f_j^2(\text{net}_j^2(N)) = \exp(-\text{net}_j^2(N)), \quad j = 1, 2, \dots, n \quad (23)$$

where $\text{net}_j^2(N) = -(y_i^1 - m_j)^2 / \sigma_j^2$, $i = 1, 2$; n is the total number of the linguistic variables with respect to the input nodes; σ_j and m_j are, respectively, the standard deviation and the mean of the Gaussian function.

Layer 3 (rule layer):

In the rule layer, each node is represented by \prod , which multiplies the input signals and outputs the result.

$$y_k^3(N) = f_k^3(\text{net}_k^3(N)) = \text{net}_k^3(N), \quad k = 1, \dots, p \quad (24)$$

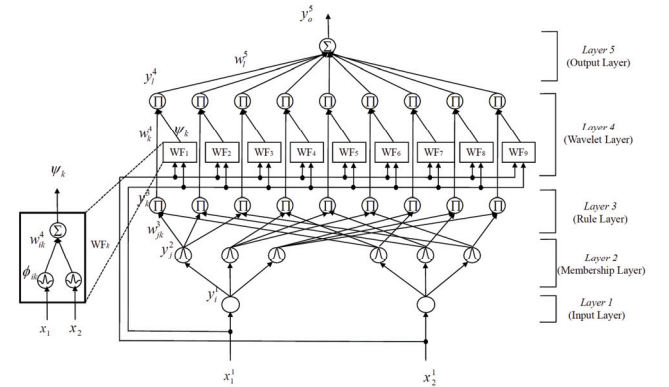


Fig. 4. Network structure of WFNN.

where $net_k^3(N) = \prod_j w_{jk}^3 y_j^2(N)$; w_{jk}^3 is the connective weight between the rule layer and the membership layer; y_j^2 is j th input to the node of layer 3.

Layer 4 (wavelet layer):

These y_k^3 signals are the input signals for the next layer, which is the wavelet layer. It includes p wavelet functions (WF_k). The WF_k are expressed as follows:

$$\psi_k = \sum w_{ik}^4 \phi_{ik}(x), i=1,2 \quad k=1, \dots, p \quad (25)$$

where $\phi_{ik}(x) = \frac{1}{\sqrt{|\sigma_j|}} \left[1 - \frac{(x_i^1 - m_j)^2}{\sigma_j^2} \right] \exp\left[-\frac{(x_i^1 - m_j)^2}{2\sigma_j^2} \right]$ and

ϕ_{ik} is i th in the k th term wavelet output to the node of wavelet sum layer; w_{ik}^4 is the wavelet weight in the WF_k layer; ψ_k is k th term WF_k output to the node of the wavelet layer.

The output signals of the l th layer are multiplied by the output of the WF_k and is represented as follows:

$$y_l^4(N) = f_l^4(net_l^4(N)) = net_l^4(N), \quad l=1, \dots, q \quad (26)$$

where $net_l^4(N) = \prod_k \psi_k w_k^4 y_k^3(N)$, $k=1, \dots, p$

Layer 5 (output layer):

In the output layer, the single node o is denoted by \sum , which calculates the overall output as the summation of all input signals

$$y_o^5(N) = f_o^5(net_o^5(N)) = net_o^5(N), \quad o=1 \quad (27)$$

where $net_o^5(N) = \sum_l w_l^5 y_l^4(N)$; y_l^4 represents the l th input to the node of layer 5; w_l^5 is the connective weight between the output layer and the wavelet layer. Moreover, $y_o^5 = \hat{W}(\Gamma)$ for the square of DC-link voltage control, $y_o^5 = i_{ds}^*(t)$ for the active power control and $y_o^5 = i_{qs}^*(t)$ for the reactive power control.

D. Compensated Controller

The minimum approximation error of the uncertainty observer is defined as follows for the development of the compensated controller:

$$\varepsilon(t) = W(t) - \hat{W}(\Gamma^*) \quad (28)$$

where Γ^* is an optimal weight vector that achieves the minimum approximation error. The absolute value of $\varepsilon(t)$ is assumed to be less than a small positive constant δ , i.e. $|\varepsilon(t)| < \delta$. From (15), (17), and (21), an error equation can be derived as follows:

$$\begin{aligned} E' &= \Lambda E + \mathbf{B}_p \{ [W(t) - \hat{W}(\Gamma)] + B_n(t) U_C(t) \} \\ &= \Lambda E + \mathbf{B}_p \{ [\hat{W}(\Gamma^*) - \hat{W}(t)] + [W(t) - \hat{W}(\Gamma^*)] + B_n(t) U_C(t) \} \quad (29) \\ &= \Lambda E + \mathbf{B}_p \{ [\mathbf{w}^{5*} - \mathbf{w}^5]^T \mathbf{y}^4 + \varepsilon(t) + B_n(t) U_C(t) \} \end{aligned}$$

where $\mathbf{w}^5 = [w_1^5 \quad w_2^5 \quad \dots \quad w_p^5]$, $\mathbf{y}^4 = [y_1^4 \quad y_2^4 \quad \dots \quad y_p^4]$, $\Lambda = \begin{bmatrix} 0 & 1 \\ -k_2 & -k_1 \end{bmatrix}$ is a stable matrix and $\mathbf{B}_p = [0 \quad -1]^T$.

Theorem 1: Considering the SCIG system represented by (13), if the hybrid WFNN control law is designed in (17), in which the computed torque control law is designed in (21), the adaptation law of the WFNN is designed in (30), and the compensated control is designed in (31), then the asymptotical stability of the control system is guaranteed.

$$(\mathbf{w}^5)' = \eta \mathbf{E}^T \mathbf{P} \mathbf{B}_p \mathbf{y}^4 \quad (30)$$

$$U_C(t) = -B_n^{-1}(t) \delta \operatorname{sgn}(\mathbf{E}^T \mathbf{P} \mathbf{B}_p) \quad (31)$$

where $\operatorname{sgn}(\cdot)$ is a sign function.

Proof: A Lyapunov function is defined as

$$V(t) = \frac{1}{2} \mathbf{E}^T \mathbf{P} \mathbf{E} + \frac{1}{2\eta} [\mathbf{w}^{5*} - \mathbf{w}^5]^T [\mathbf{w}^{5*} - \mathbf{w}^5] \quad (32)$$

where η is a positive constant, and \mathbf{P} is a symmetric positive definite matrix which satisfies the following Lyapunov equation:

$$\Lambda^T \mathbf{P} + \mathbf{P} \Lambda = -\mathbf{Q} \quad (33)$$

and $\mathbf{Q} > 0$ is selected by the designer. Take the derivative of the Lyapunov function and use (28), (29), and (33), then

$$\begin{aligned} V'(t) &= \frac{1}{2} \mathbf{E}^T \mathbf{P} E' + \frac{1}{2} \mathbf{E}^T \mathbf{P} E - \frac{1}{\eta} [\mathbf{w}^{5*} - \mathbf{w}^5]^T (\mathbf{w}^5)' \\ &= \frac{1}{2} \mathbf{E}^T \mathbf{P} \Lambda E + \frac{1}{2} \mathbf{E}^T \Lambda^T \mathbf{P} E + \mathbf{E}^T \mathbf{P} \mathbf{B}_p \{ [\mathbf{w}^{5*} - \mathbf{w}^5]^T \mathbf{y}^4 \\ &\quad + \varepsilon(t) + B_n(t) U_C(t) \} - \frac{1}{\eta} [\mathbf{w}^{5*} - \mathbf{w}^5]^T \mathbf{w}' \quad (34) \\ &= \frac{1}{2} \mathbf{E}^T \mathbf{Q} E + \mathbf{E}^T \mathbf{P} \mathbf{B}_p [\varepsilon(t) + B_n(t) U_C(t)] \\ &\quad + \mathbf{E}^T \mathbf{P} \mathbf{B}_p [\mathbf{w}^{5*} - \mathbf{w}^5]^T \mathbf{y}^4 - \frac{1}{\eta} [\mathbf{w}^{5*} - \mathbf{w}^5]^T (\mathbf{w}^5)' \end{aligned}$$

To satisfy $V'(t) \leq 0$, the update law $(\mathbf{w}^5)'$ and the compensated controller $U_C(t)$ are designed as (30) and (31). Substitute (30) into (34) and use (31), then

$$\begin{aligned} V'(t) &= -\frac{1}{2} \mathbf{E}^T \mathbf{Q} E + \mathbf{E}^T \mathbf{P} \mathbf{B}_p \varepsilon(t) + \mathbf{E}^T \mathbf{P} \mathbf{B}_p B_n(t) U_C(t) \\ &\leq -\frac{1}{2} \mathbf{E}^T \mathbf{Q} E + \left| \mathbf{E}^T \mathbf{P} \mathbf{B}_p \right| |\varepsilon(t)| + \mathbf{E}^T \mathbf{P} \mathbf{B}_p B_n(t) U_C(t) \quad (35) \\ &\leq -\frac{1}{2} \mathbf{E}^T \mathbf{Q} E \leq 0 \end{aligned}$$

Since $V'(t) \leq 0$, $V(t)$ is negative semidefinite (i.e., $V(t) \leq V(0)$), which implies \mathbf{E} and $[\mathbf{w}^{5*} - \mathbf{w}^5]^T$ are bounded. Define function $\Theta(t) = \frac{1}{2} \mathbf{E}^T \mathbf{Q} \mathbf{E} \leq -V'(t)$, and integrate function $\Theta(t)$ with respect to time

$$\int_0^t \Theta(\tau) d\tau \leq V(0) - V(t) \quad (36)$$

Because $V(0)$ is bounded, and $V(t)$ is nonincreasing and bounded, then

$$\lim_{t \rightarrow \infty} \int_0^t \Theta(\tau) d\tau \leq \infty \quad (37)$$

Differentiate with respect to time

$$\Theta'(t) = \mathbf{E}^T \mathbf{Q} \mathbf{E}' \quad (38)$$

Since all the variables in the right-hand side of (29) are bounded, it implies \mathbf{E}' is also bounded. Then $\Theta'(t)$ is uniformly continuous. By using the Barbalat's lemma, it can be shown that $\lim_{t \rightarrow \infty} \Theta(t) = 0$. Thus, $\mathbf{E} \rightarrow 0$ as $t \rightarrow \infty$. As a result, the hybrid WFNN control system is asymptotically stable.

E. Online Parameters Learning

The supervised learning algorithms are adopted for the parameters learning to adjust the connective weights in the output and wavelet layers, and the parameters of membership functions using the BP algorithm to minimize a given energy function.

Layer 5:

The update law shown in (30) can be redescribed as follows:

$$(\mathbf{w}^5)' = \eta \mathbf{E}^T \mathbf{P} \mathbf{B}_p \mathbf{y}^4 \equiv \eta e' \mathbf{y}^4 \quad (39)$$

In this layer, the update law of the weights can be obtained as follows according to the gradient descent method:

$$(\mathbf{w}^5)' = \eta e' \mathbf{y}^4 = -\eta \frac{\partial V}{\partial y_o^5} \frac{\partial y_o^5}{\partial w_l^5} = -\eta \frac{\partial V}{\partial y_o^5} \mathbf{y}^4 \quad (40)$$

Layer 4:

The error term to be propagated is given by:

$$\delta_l^4 = -\frac{\partial V}{\partial y_l^4} = e' w_l^5 \quad (41)$$

Layer 3:

The error term is calculated as follows:

$$\delta_k^3 = -\frac{\partial V}{\partial y_k^3} = e' w_l^5 w_k^4 \psi_k \quad (42)$$

By using the chain rule, the weight is updated by the amount:

$$\Delta w_{ik}^4 = -\eta_w \frac{\partial V}{\partial w_{ik}^4} = \begin{cases} \eta_w e' w_l^5 y_k^3 w_k^4 \phi_{1k}, & i = 1 \\ \eta_w e' w_l^5 y_k^3 w_k^4 \phi_{2k}, & i = 2 \end{cases} \quad (43)$$

Layer 2:

In this layer, the error term to be propagated is given by:

$$\delta_j^2 = -\frac{\partial V}{\partial y_j^2} = e' w_l^5 w_k^4 \psi_k \frac{\partial y_k^3}{\partial y_j^2} \quad (44)$$

Also, the update laws of means and standard deviations of the Gaussian function are:

$$\Delta m_j = -\eta_m \frac{\partial V}{\partial m_j} = \eta_m e' w_l^5 w_k^4 \psi_k \frac{\partial y_k^3}{\partial y_j^2} y_j^2 \frac{(-2)(m_j - y_j^1)}{\sigma_j^2} \quad (45)$$

$$\Delta \sigma_j = -\eta_\sigma \frac{\partial V}{\partial \sigma_j} = \eta_\sigma e' w_l^5 w_k^4 \psi_k \frac{\partial y_k^3}{\partial y_j^2} y_j^2 \frac{(2)(y_j^1 - m_j)^2}{\sigma_j^3} \quad (46)$$

where η_{w1} , η_{w2} , η_σ and η_m are the learning rates of the connective weights, standard deviations and means respectively.

F. Stability Analysis Using Projection Algorithm

By using Theorem 1, the stability proof of the hybrid WFNN control system which is based on the assumption of the bound of the minimum approximation error can be guaranteed. However, the convergence condition of the WFNN has to be satisfied. If the parameters of the WFNN are bounded, the convergence property of the WFNN can be guaranteed. Moreover, from (27) the output of the WFNN is bounded if the weights between the output layer and the wavelet layer are bounded. Define the constrain set Ω_b for \mathbf{w}^5 as:

$$\Omega_b = \{\|\mathbf{w}^5\| \leq M_b\} \quad (47)$$

where M_b is the upper bound of \mathbf{w}^5 and $\|\cdot\|$ is a two-norm of vector. Hence, by using the projection algorithm [10], the update law (39) is modified as follows to guarantee $\mathbf{w}^5 \in \Omega_b$:

$$(\mathbf{w}^5)' = \begin{cases} \eta \mathbf{E}^T \mathbf{P} \mathbf{B}_p \mathbf{y}^4 & \text{if } \|\mathbf{w}^5\| \leq M_b \text{ or } (\|\mathbf{w}^5\| = M_b \text{ and } \mathbf{E}^T \mathbf{P} \mathbf{B}_p \mathbf{w}^{5T} \mathbf{y}^4 \leq 0) \\ \eta \mathbf{E}^T \mathbf{P} \mathbf{B}_p \mathbf{y}^4 - \eta \mathbf{E}^T \mathbf{P} \mathbf{B}_p \frac{\mathbf{w}^5 \mathbf{w}^{5T} \mathbf{y}^4}{\|\mathbf{w}^5\|^2} & \text{if } (\|\mathbf{w}^5\| = M_b \text{ and } \mathbf{E}^T \mathbf{P} \mathbf{B}_p \mathbf{w}^{5T} \mathbf{y}^4 > 0) \end{cases} \quad (48)$$

The convergence property of the WFNN can be guaranteed according to the projection algorithm. Thus, the minimum approximation error which is bounded can be reasonable to be assumed. Furthermore, to achieve the best transient control

performance considering the possible variation of operating conditions of the hybrid WFNN control system, the bound of the approximation error δ shown in (31) is chosen. In addition, the asymptotical stability of the proposed hybrid WFNN control system using the projection algorithm can be shown by the following theorem.

Theorem 2: Considering the SCIG system shown in (13), if the hybrid WFNN control law is designed in (17), in which the computed torque control law is designed in (21), the adaptation law of the WFNN is designed in (48), and the compensated control is designed in (31), then the asymptotical stability of the control system is guaranteed.

V. EXPERIMENTAL RESULTS

The block diagram and photos of the computer controlled SCIG system is shown in Fig. 5. The block diagram of the personal computer (PC)-based control computer, including two MRC-6810 servo control cards for the control of AC/DC and DC/AC power converters respectively, for the intelligent hybrid WFNN controlled SCIG system is shown in Fig. 5(a). The values of the DC-link capacitor C_{dc} and the filter inductor L are $1400 \mu F$ and $10mH$ respectively. Moreover, the photos of PC-based control computer, SCIG set and PMSM as the prime mover are shown in Fig. 5(b). The indirect field-oriented control algorithm, synchronization algorithm, the hybrid WFNN controller and the WFNN controllers are realized in a PC via the Simulink Real-Time Control package.

In order to verify the control performance of the proposed intelligent hybrid WFNN controlled SCIG system, one case as follows with the flux control current i_{ds}^* 5.4A and step command of $(V_{dc}^*)^2 = 57600 V^2$ (DC-link voltage 240V) is tested to demonstrate the control performance of the SCIG system: varying rotor speed to emulate varying wind speed condition. Moreover, in the varying speed test case, the rotor speed is changed from 1054rpm ($v=8m/s$) to 790rpm ($v=6m/s$) to 1054rpm ($v=8m/s$) to 1318rpm ($v=10m/s$) to 1186rpm ($v=9m/s$) and finally changed to 1581rpm ($v=12m/s$). Furthermore, to compare the control performance of the hybrid WFNN controller, the experimental results using the ideal computed torque controller shown in (19), where the term $W(t)$ is set to zero due to unavailable value of the lumped uncertainty, are also discussed.

In the experimentation, first, the experimental results using the ideal computed torque controller for the AC/DC power converter and the WFNN controllers for the DC/AC power inverter at the test condition of varying rotor speed are shown in Fig. 6. The responses of the square of DC-link voltage V_{dc}^2 , active power P and reactive power Q are shown in Figs. 6(a)-(c) respectively. From the experimental results, poor tracking responses of the square of DC-link voltage V_{dc}^2 under varying rotor speed as shown in Fig. 6(a) is owing to the unknown of the real value of the $W(t)$ of the SCIG

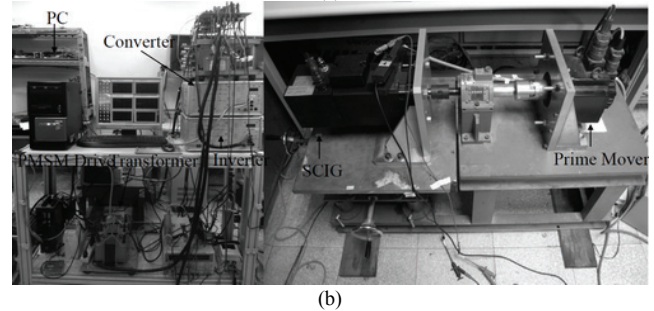
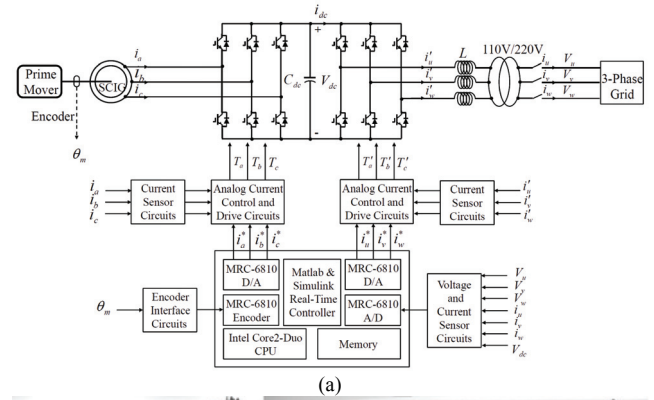


Fig. 5. Computer controlled SCIG system. (a) Computer control system. (b) Photos of PC-based control computer, SCIG set and prime mover.

system using the ideal computed torque controller. Moreover, the experimental results using the proposed hybrid WFNN controller for the AC/DC power converter and the WFNN controller for the DC/AC power inverter at the test condition of varying rotor speed are shown in Fig. 7. The responses of the square of DC-link voltage V_{dc}^2 , active power P and reactive power Q are shown in Figs. 7(a)-(c) respectively. From the experimental results, the steady-state control performance using the ideal computed torque controller as shown in Fig. 6(a) is much improved by the proposed hybrid WFNN controller as shown in Fig. 7(a) due to the powerful approximated ability of the WFNN uncertainty observer and the effective compensation of the compensated controller. Thus, the adaptive and robust control characteristics of the proposed hybrid WFNN control system can be clearly observed.

VI. CONCLUSIONS

This study successfully demonstrated the development and implementation of the intelligent hybrid WFNN controller for the square of DC-link voltage command tracking of a SCIG system for grid-connected wind power applications using power converters. First, the mathematical model of the SCIG system was introduced. Then, the theoretical bases of the ideal computed torque controller, WFNN uncertainty observer, compensated controller and online parameters learning of the WFNN were described in detail. Moreover, the experimentation was carried out to test the effectiveness of the proposed hybrid WFNN control. From the experimental results, the control performance of the proposed hybrid WFNN controlled SCIG system is adaptive with

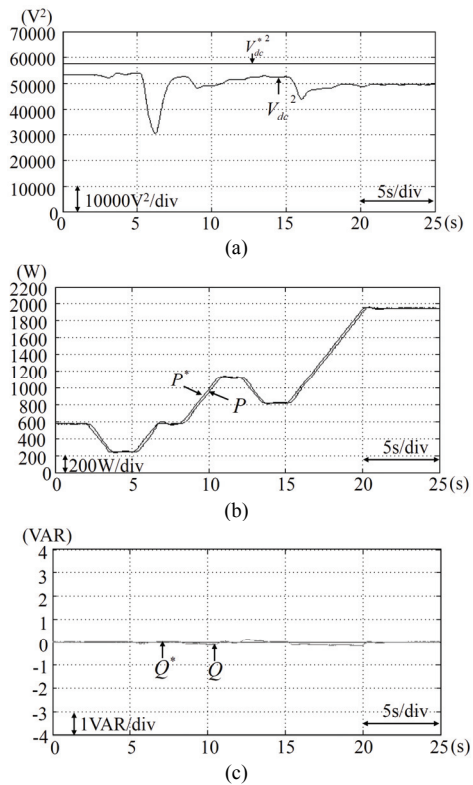


Fig. 6. Experimental results of ideal computed torque controlled SCIG system at varying rotor speed. (a) Tracking response of square of DC-link voltage. (b) Tracking response of active power. (c) Tracking response of reactive power.

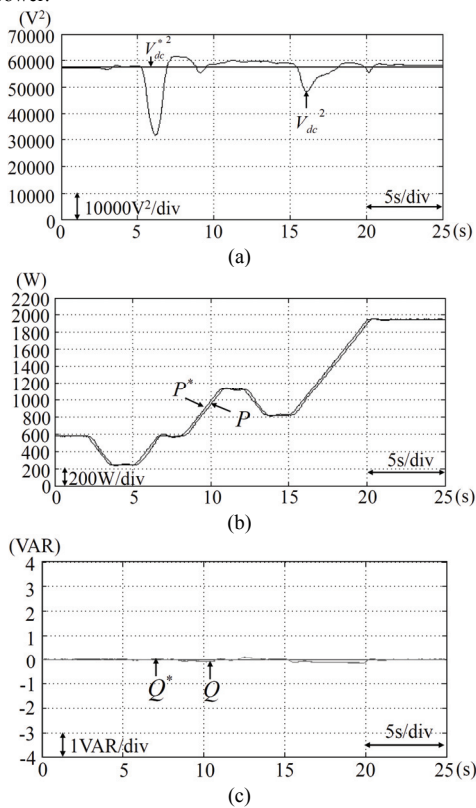


Fig. 7. Experimental results of hybrid WFNN controlled SCIG system at varying rotor speed. (a) Tracking response of square of DC-link voltage. (b) Tracking response of active power. (c) Tracking response of reactive power.

regard to the operating condition of the SCIG.

REFERENCES

- [1] Z. Xu, Q. Hu, and M. Ehsani, "Estimation of effective wind speed for fixed-speed wind turbines based on frequency domain data fusion," *IEEE Trans. Sustainable Energy*, vol. 3, no. 1, pp. 57-64, January 2012.
- [2] L. Y. Pao and K. E. Johnson, "Control of wind turbines," *IEEE Control System*, vol. 31, no. 2, pp. 44-62, April 2011.
- [3] L. Qu and W. Qiao, "Constant power control of DFIG wind turbines with supercapacitor energy storage," *IEEE Trans Industrial Applications*, vol. 47, no. 1, pp. 359-367, 2011.
- [4] F. J. Lin, M. S. Huang, P. Y. Yeh, H. C. Tsai, and C. H. Kuan, "DSP-based probabilistic fuzzy neural network control for Li-Ion battery charger," *IEEE Trans. Power Electron*, vol. 27, no. 8, pp.3782-3794, August 2012.
- [5] W. M. Lin and C. M. Hong, "A new Elman neural network-based control algorithm for adjustable-pitch variable-speed wind-energy conversion systems," *IEEE Trans. Power Electron*, vol. 26, no.2, pp.473-481, February 2011.
- [6] Y. Song and L. Gao, "Incremental battery model using wavelet-based neural networks," *IEEE Trans. Components, Packaging and Manufacturing Technology*, vol. 1, no. 7, pp.1075-1081, July 2011.
- [7] F. J. Lin, K. H. Tan, and J. H. Chiu, "Active islanding detection method using wavelet fuzzy neural network," In *Proc. 2012 IEEE int. Conf. Fuzzy Systems*, Brisbane, 2012, pp 1-8.
- [8] F. J. Lin, L. T. Teng, P. H. Shieh, and Y. F. Li, "Intelligent controlled wind turbine emulator and induction generator system using RBFN," *IET Proc. Electric Power Applications*, vol. 153, no. 4, pp.608-618, July 2006.
- [9] R. Teodorescu and F. Blaabjerg, "Flexible control of small wind turbines with grid failure detection operating in stand-alone and grid-connected mode," *IEEE Trans. Power Electron*, vol.19, no. 5, pp.1323-1332, September 2004.
- [10] F. J. Lin, R. J. Wai, and C. M. Hong, "Hybrid supervisory control using recurrent fuzzy neural network for tracking periodic inputs," *IEEE Trans. Neural Networks*, vol. 12, no. 1, pp.68-90, August 2001.